Journal of Applied Remote Sensing

RemoteSensing.SPIEDigitalLibrary.org

Large-scale radiation and energy balances with Landsat 8 images and agrometeorological data in the Brazilian semiarid region

Antônio Heriberto de Castro Teixeira
Janice Freitas Leivas
Fernando Braz Tangerino Hernandez
Renato Alberto Momesso Franco

SPIE.

Antônio Heriberto de Castro Teixeira, Janice Freitas Leivas, Fernando Braz Tangerino Hernandez, Renato Alberto Momesso Franco, "Large-scale radiation and energy balances with Landsat 8 images and agrometeorological data in the Brazilian semiarid region," *J. Appl. Remote Sens.* **11**(1), 016030 (2017), doi: 10.1117/1.JRS.11.016030.

Large-scale radiation and energy balances with Landsat 8 images and agrometeorological data in the Brazilian semiarid region

Antônio Heriberto de Castro Teixeira,[a,*] Janice Freitas Leivas,[a] Fernando Braz Tangerino Hernandez,[b] and Renato Alberto Momesso Franco[b]

[a]Embrapa Satellite Monitoring, Campinas, São Paulo, Brazil
[b]São Paulo State University, Department of Hydrology, Ilha Solteira, São Paulo, Brazil

Abstract. Aiming to subsidize the rational water resources management, four Landsat 8 (L8) images along different conditions of the year 2014 were used for modeling the radiation and energy balances in the mixed agroecosystems inside a Brazilian reference semiarid area. The SAFER algorithm was applied to calculate the latent heat flux (λE); net radiation (R_n) was acquired by the Slob equation; ground heat flux (G) was considered a fraction of R_n; and the sensible heat flux (H) was retrieved by residue in the energy balance equation. For classifying the vegetation, the surface resistance algorithm (SUREAL) was used to estimate the surface resistance to the water fluxes (r_s) with threshold values for r_s. Clearly, one could see higher λE values from irrigated crops (ICs) than those for natural vegetation (NV) with some situations of heat horizontal advection. The respective λE, H, and G average ratios to R_n for the ICs ecosystem were 64% to 79%, 18% to 28%, and 3%, respectively. For the NV ecosystem, the corresponding fractions were 4% to 37%, 60% to 94%, and 4%, respectively. The algorithms proved to have strong sensibility to quantifying the large-scale energy and mass exchanges by applying L8 images in mixed agroecosystems of semiarid environments. [DOI: 10.1117/1.JRS.11.016030]

Keywords: net radiation; latent heat flux; sensible heat flux; soil heat flux; energy partition.

Paper 16519P received Jul. 7, 2016; accepted for publication Jan. 4, 2017; published online Feb. 22, 2017.

1 Introduction

Energy exchanges in semiarid regions have gained notoriety due to their agroecosystem dynamics and impacts on regional and local climates. The Petrolina County, Pernambuco state, in the Brazilian semiarid, is an example. Nowadays, it is highlighted as an important agricultural growing region because of the irrigation technologies applied to fruit crops at the vicinities of the São Francisco River. Under these rapid land-use changing conditions, the use of remote sensing by satellite images is strongly relevant for large-scale quantification of the energy and mass exchanges between the surface and the lower atmosphere and is the method used in distinct environments around the world.[1–4]

After taking into account all the radiation balance components, the net radiation (R_n) is the difference between incoming and outgoing radiation fluxes of both short and long wavelengths. R_n is partitioned into latent (λE), sensible (H), and ground (G) heat fluxes.[5] Other energy terms, such as heat stored or released in/from the canopies or the energy used in metabolic activities, are in general not considered because they account only for a small fraction of the daily R_n and may be neglected in environmental studies.[6]

The use of remote sensing by satellite images is a suitable way for determining and mapping the spatial and temporal structure of the radiation and energy balance components. Several

*Address all correspondence to: Antônio Heriberto de Castro Teixeira, E-mail: heriberto.teixeira@embrapa.br

1931-3195/2017/$25.00

algorithms have been developed for this task, with some advantages and shortcomings, such as, the surface energy balance algorithm for land (SEBAL),[7] the surface energy balance index (S-SEBI),[8] and the surface energy balance system (SEBS).[9]

Although SEBAL had been calibrated and validated with field radiation and energy balance measurements, and presented a good performance in the Brazilian semiarid region,[10,11] the major difficult in its applicability is the need for an anchor dry pixel for neglecting λE. During the rainy season in this region, the mixed agroecosystems composed of irrigated crops (ICs) and natural vegetation (NV) are homogenously wet, all presenting high water fluxes, with λE values from the natural "Caatinga" species being even larger than those from irrigation plots in some occasions.[6]

Another problem in relation to the applicability of some remote sensing radiation and energy balance algorithms, when aiming at the end users, is the need for background knowledge in radiation physics. The use of the Penman–Monteith (PM) equation has been suggested for applying remotely sensed vegetation indices, such as the normalized difference vegetation index (NDVI) and the enhanced vegetation index, together with weather data.[12,13] The PM equation is also highlighted by both the use of the crop coefficient (K_c) approach[5,14] and the model named mapping evapotranspiration with high-resolution and internalized calibration (METRIC).[15]

Considering the simplicity of the PM equation for large-scale applications, two algorithms based on this equation were developed and validated under the Brazilian semiarid conditions.[1] They are called simple algorithm for evapotranspiration retrieving (SAFER), which is based on the modeled ratio of the actual (ET) to the reference (ET_0) evapotranspiration to acquire λE, and surface resistance algorithm (SUREAL) for estimating the surface resistance to the water fluxes (r_s). This last model has been successfully applied for classifying ICs and NV in the mixed Brazilian semiarid agroecosystems.[6] To elaborate and validate these algorithms, field data from four flux stations were used together with satellite images involving ICs and NV agroecosystems under strong contrasting thermohydrological and surface cover conditions over several years.[1,16]

Hernandez et al.[17] compared the SAFER and SEBAL algorithms with the K_c approach[5] in the Northwestern side of the São Paulo state, Brazil. These applications were done on corn, beans, and sugarcane crops that were irrigated by center pivots. According to the authors, SAFER presented better performance than SEBAL under the conditions of low soil cover by the canopies.

The Landsat 8 (L8) satellite was launched on February 11, 2013, and normal operations started on May 30, 2013. It has a 16-day ground track repeat cycle with an equatorial crossing time at 10:00 a.m. The Operational Land Imager on L8 is a nine-band push broom scanner with a swath width of 185 km.[18] Some radiation and energy balance studies using remote sensing data have been carried out in the Brazilian semiarid region but with limitations of free-cloud cover images with just one Landsat 5/7 image in a year. However, new research is needed to test the suitability of the L8 satellite for these studies, especially with the availability of images covering different seasons as in the case of the current paper. These new studies are important for operationally monitoring the energy exchanges among the different agroecosystems to assist large-scale water management.[19]

The objective of the current research is to apply the SAFER and SUREAL algorithms with L8 images together with a net of agrometeorological stations, covering different seasons of the year 2014, aiming to quantify the large-scale radiation and energy balance components. The results can subsidize criteria for policy decisions aimed at rational water resources management under conditions of rapid land-use and climate changes together with water competitions among different sectors. The success of the modeling with the L8 satellite images may give more confidence for testing and validating the algorithms in other environments around the world, which probably will only need calibrations of the original equations.

2 Material and Methods

2.1 *Study Area and Dataset*

Figure 1 shows the location of the reference semiarid area (dashed red square on the right side) inside the Petrolina County, Pernambuco state, Northeast of Brazil, together with the net of seven

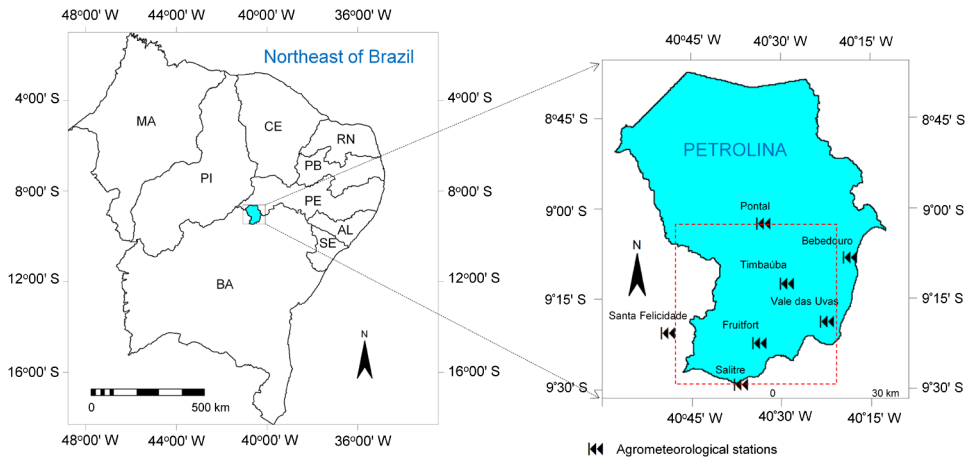

Fig. 1 Location of the reference semiarid area (dashed red square on the right side) inside the Petrolina County, Pernambuco state, Northeast Brazil and the agrometeorological stations used for the weather data interpolation processes in a GIS environment.

agrometeorological stations (black arrows) used for the weather data interpolation processes in a geographic information system (GIS) environment.

According to Teixeira,[20] in the reference semiarid area shown in Fig. 1, excluding a very few high-altitude places, all the flat areas present long-term annual air temperature (T_a) higher than 24°C. The average monthly maximum value is 33°C and the minimum is 19°C. The warmest months are October and November when the sun is around the zenith position with low cloud cover, while the coldest months are June and July, at the winter solstice in the south hemisphere. The thermal homogeneity strongly contrasts with the spatial and temporal heterogeneity of the rainfall regime. Most rains fall during the first four months of the year, accounting for 68% of the annual total, which presents a long-term (50 years) value of 570 mm yr^{-1} registered at the "Bebedouro" station (see Fig. 1). The sandy soil is classified as Latossoil red-yellow with low retention capacity with a groundwater depth of around 2.5 m.

The ICs agroecosystem is composed mainly of fruit crops, with the main ones being grapes, mangos, guava, and bananas, surrounded by the NV ecosystem ("Caatinga"). The "Caatinga" species are defined as bushes that possess small leaves or thorns. During the dry seasons they become senescent; however, as soon as the rains start, the plants rapidly turn green. Some of them lose their leaves in the dry periods, and others store water, being adapted to tolerate water stress and thrive under environmental constraints, which increases their rainfall water productivity.

Data from seven agrometeorological stations (see Fig. 1) were used together with four L8 images acquired under different thermohydrological conditions in the year 2014 [day of the year (DOY): 25—January, 25; 153—June, 2; 217—August, 5; and 265—September, 22]. Grids of global solar radiation (R_G), T_a, and ET_0 from the stations were used together with the remotely sensed retrieved parameters during the modeling steps for the large-scale radiation and energy balance components estimations.[6] The grids of weather data with the same pixel sizes of the L8 images were constructed using the "moving average" interpolation method in a GIS environment.

2.2 *Large-Scale Radiation and Energy Balances Modeling*

Figure 2 presents the flowchart for the large-scale radiation and energy balance modeling, using L8 images together with agrometeorological data through the SAFER algorithm. The bands 1 to 7 (spatial resolution of 30 m) were used to calculate the surface albedo (α_0), bands 4 and 5 were used to retrieve NDVI, and the surface temperature (T_0) was estimated using the bands 10 and 11 (spatial resolution of 100 m).

All the regression coefficients of the equations for acquiring the parameters in Fig. 2 were determined in the reference semiarid area shown in Fig. 1 with simultaneous Landsat satellite

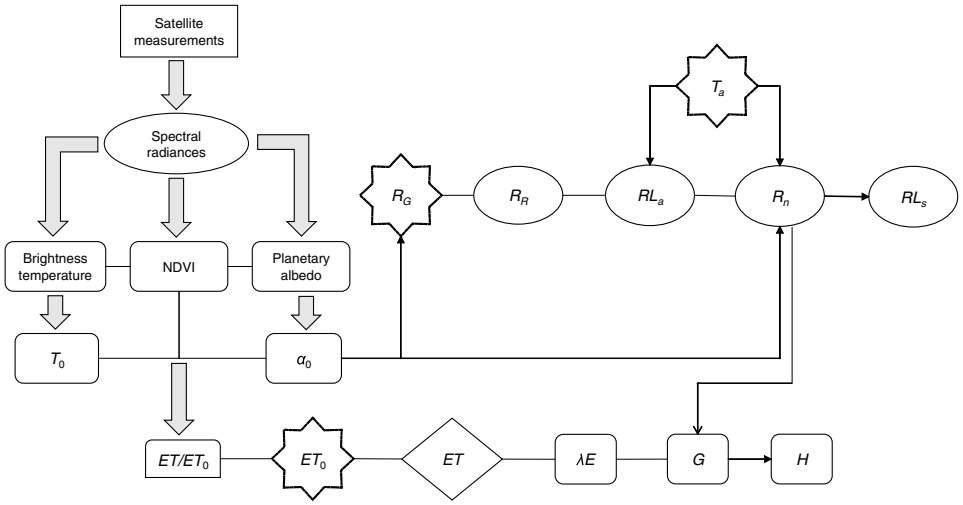

Fig. 2 Flowchart for the large-scale radiation and energy balances by applying the SAFER using L8 images together with agrometeorological data.

and field measurements, involving strongly contrasting agroecosystems and under different thermohydrological conditions throughout several years.[1,6,10,16]

Following Fig. 2, the spectral radiances (L_b) were computed from digital numbers (DN)

$$L_b = \text{Gain}\, x\, \text{DN} + \text{Offset}, \tag{1}$$

where Gain and Offset refer to the values given in the Landsat metadata file.[18]

The planetary albedo for each Landsat satellite band (αp_b) was calculated as

$$\alpha p_b = \frac{L_b \pi d^2}{Ra_b \cos \varphi}, \tag{2}$$

where L_b is the spectral radiance for the wavelengths of band b ($\text{W m}^{-2}\,\text{sr}^{-1}\,\mu\text{m}^{-1}$), d is the relative earth–sun distance, Ra_b is the mean solar irradiance at the top of the atmosphere (or atmospheric irradiance) for each band ($\text{W m}^{-2}\,\mu\text{m}^{-1}$), and φ is the solar zenith angle.[6]

Ra_b for each of the L8 bands 1 to 7 was calculated according to Planck's law, integrating the radiation over the wavelength intervals and considering their fractions over the solar spectrum, assuming the sun as a blackbody. Then, the broadband planetary albedo (α_p) was obtained as the total sum of the different narrow-band αp_b values according to their weights (w_b)

$$\alpha p = \sum w_b \alpha p_b, \tag{3}$$

where the w_b values were computed as the ratio of the amount of the incoming shortwave (sw) radiation from the sun at the top of the atmosphere in a particular band and the sum for all the bands.

Table 1 shows the wavelengths, Ra_b and w_b for each of the bands used (B1–B7) in the α_p calculations from the spectral L8 measurements.

The spectral radiances from the L8 bands 10 (L_{10}) and 11 (L_{11}) were converted into radiometric temperatures applicable at the top of the atmosphere (T_b) by inversion of the Planck's law in the 10.6- to 11.19-μm (band 10) and 11.5- to 12.51-μm (band 11) bandwidth

$$T_b = \frac{K_2}{\ln\left(\frac{K_1}{L_b+1}\right)}, \tag{4}$$

where K_1 (774.89 and 480.89) and K_2 (1321.08 and 1201.14) for bands 10 and 11, respectively, are conversion coefficients for the L8 satellite.

Table 1 Radiometric parameters for the planetary albedo (α_p) calculations from the L8 images: wavelengths of the bands—λ_b; mean solar irradiance at the top of the atmosphere for each band—Ra_b; and the weights for each band—w_b.

L8 parameter	B1	B2	B3	B4	B5	B6	B7
λ_b (μm)	0.43 to 0.45	0.45 to 0.51	0.53 to 0.59	0.64 to 0.67	0.85 to 0.88	1.57 to 1.65	2.11 to 2.29
Ra_b (W m^{-2} μm^{-1})	1718.8	1810.4	1741.7	1558.3	962.5	206.3	68.8
w_b	0.10	0.31	0.30	0.13	0.08	0.05	0.04

The average T_b value from the two bands was considered the brightness temperature (T_{bright}); however, conditional functions were used when one of the bands 10 or 11 presented pixel value problems to retrieve only one band Planck's result for T_{bright}.

Both α_p and T_{bright} were corrected atmospherically for acquiring the surface instantaneous values of albedo (α_0) and temperature (T_0) by regression equations determined from previous simultaneous Landsat and field measurements. Another regression between the instantaneous and daily values was also applied to upscale the satellite overpass to the 24-hour α_0 and T_0 values.[1,6,10,16]

NDVI is a land cover and water-related indicator obtained from satellite images as

$$\text{NDVI} = \frac{\alpha p_{(\text{nir})} - \alpha p_{(\text{red})}}{\alpha p_{(\text{nir})} + \alpha p_{(\text{red})}}, \tag{5}$$

where αp_{nir} and αp_{red} represent the planetary albedo over the wavelength ranges in the near-infrared (subscript nir) and red (subscript red) regions of the solar spectrum, which for the L8 satellite are the bands 5 (B5) and 4 (B4), respectively (see Table 1).

Daily R_n was calculated using the Slob equation[7,16,20,21]

$$R_n = (1 - \alpha_0)R_G - a_L \tau_{\text{sw}}, \tag{6}$$

where τ_{sw} is the sw atmospheric transmissivity calculated as the ratio of R_G to the incident solar radiation at the top of the atmosphere (R_a) and the regression coefficient a_L was spatially distributed through its relationship with T_a[20]

$$a_L = aT_a - b, \tag{7}$$

A constant value for $a_L = 110$ was previously used without considering the thermal spatial differences.[7]

The atmospheric longwave radiation (RL_a) was calculated by applying the Stefan–Boltzmann law

$$RL_a = \sigma \varepsilon_A T_a^4, \tag{8}$$

where ε_A was estimated as follows:[1,6,10,16]

$$\varepsilon_A = a_A(-\ln \tau_{\text{sw}})^{b_A}, \tag{9}$$

where the regression coefficients a_A and b_A of 0.94 and 0.11 are between those for Idaho[22] ($a_A = 0.85$ and $b_A = 0.09$) and for Egypt[7] ($a_A = 1.08$ and $b_A = 0.26$).

Estimating the reflected solar radiation (R_R) as the product of R_G by α_0, the daily longwave surface radiation (RL_s) was retrieved as residue in the radiation balance equation

$$R_R = \alpha_0 R_G, \tag{10}$$

$$RL_s = R_G - R_R + RL_a - R_n. \tag{11}$$

Applying the SAFER algorithm, the ratio of the actual (ET) to the reference (ET_0) evapotranspiration, ET_r, was modeled at the satellite overpass time

$$ET_r = \exp\left[a_{sf} + b_{sf}\left(\frac{T_0}{\alpha_0 \text{NDVI}}\right)\right], \tag{12}$$

where a_{sf} and b_{sf} are the regression coefficients for the reference semiarid area.[1,6]

The ET_0 daily grids were obtained by applying the PM method[5] interpolating the weather data from the agrometeorological stations (black arrows on Fig. 1), and then multiplied by the images resulting from Eq. (12), giving the large-scale daily ET pixel values, which were transformed into energy units to retrieve λE

$$ET = ET_r ET_0. \tag{13}$$

Equation (12) does not work for water bodies, i.e., when NDVI < 0. Thus, the concept of equilibrium evapotranspiration (ET_{eq})[23] is adopted under these conditions in the SAFER algorithm, and λE_{eq} is retrieved through conditional functions applied to the NDVI values as

$$\lambda E_{eq} = \frac{s(R_n - G)}{s + \gamma}, \tag{14}$$

where s is the slope of the curve relating saturation water vapor pressure to T_a and γ is the psychometric constant. Under these conditions, as the surface moisture availability is not constrained, water vapor transfer is only limited by the available energy.

For the daily G values, the following equation was used:[1,6]

$$\frac{G}{R_n} = a_G \exp(b_G \alpha_0), \tag{15}$$

where a_G and b_G are regression coefficients for the reference semiarid region.

The sensible heat flux (H) was estimated as residue in the energy balance equation[19]

$$H = R_n - \lambda E - G. \tag{16}$$

For classification of the vegetated surface into ICs and NV ecosystems, the SUREAL model was applied[1,24]

$$r_s = \exp\left[a_r\left(\frac{T_0}{\alpha_0}\right)(1 - \text{NDVI}) + b_r\right], \tag{17}$$

where a_r and b_r are regression coefficients for the reference semiarid region.

Pixels with r_s values below 800 s m^{-1} and NDVI above or equal to 0.40 were considered the ICs agroecosystem. If r_s was between 1000 and 10,000 s m^{-1}, the pixels should be the NV ecosystem. The high end of this last range was used to exclude human-built structures.

3 Results and Discussion

3.1 *Weather Drivers*

The weather-driving forces for the radiation and energy balances are R_G, precipitation (P), and the atmospheric demand represented by ET_0. These parameters were analyzed on a daily scale during the transition periods comprising the start of the rainy season in 2013 to the end of the dry season in 2014, involving the previous, current, and post-thermohydrological conditions of the satellite image acquisition dates (January to September of 2014).

Figure 3 shows the daily trends of R_G, P, and ET_0 in terms of DOY with weather data from the "Timbaúba" agrometeorological station, located in the center of the reference semiarid area inside the Petrolina County, Brazilian Northeast region (see Fig. 1).

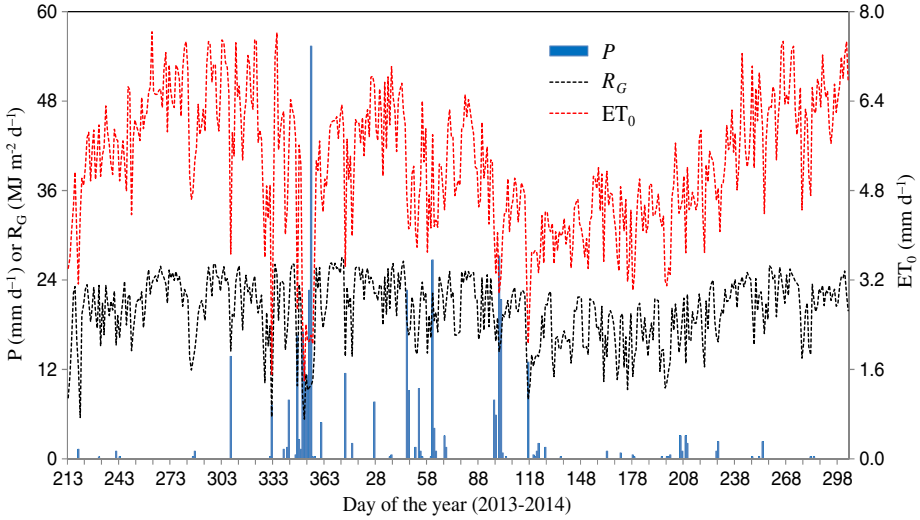

Fig. 3 Trends of the daily values of precipitation (P), incident global solar radiation (R_G), and reference evapotranspiration (ET_0), involving the DOY from the start of the rainy period in November/2013 to the end of the dry period in October/2014, in the reference semiarid area of Petrolina County, Brazilian Northeast region.

Among the analyzed weather parameters, P was the most variable in the study period. The rain concentrations were from DOY/year 303/2013 to 120/2014 (November to April), mainly at the end of 2013. The climatically driest periods, with P below 5 mm d^{-1}, were from DOY 210 to 300 of 2014 (August to October).

Analyzing the daily atmospheric demands, the largest ET_0 values happened between DOY 242 and 304 of 2014 (September to October), when they reached around 7.0 mm d^{-1}. In these situations, the sun was at the zenith position under low cloud cover conditions. The R_G daily values were higher than 25 MJ m^{-2} d^{-1} at the end of both years and below 10 MJ m^{-2} d^{-1} in the middle of 2014, with these levels significantly related to the sun astronomical positions.

Under conditions of high P, ET_0, and R_G in the second half of the year, both NV and ICs agroecosystems are in favor of large water fluxes; however, with absence of rains, only the ICs will present high rates, promoting strong hydrological contrast when compared with the natural "Caatinga" species.

3.2 *Remote Sensing Modeling Input Parameters*

The radiation and energy balances among the different agroecosystems and thermohydrological conditions will depend on α_0, NDVI, and T_0. The first parameter determines the sw radiation that comes back from the surface to the lower atmosphere. NDVI is a key remote sensing indicator related to the land cover and soil moisture, and the emitted longwave radiation is directly proportional to T_0.

The spatial distributions for the daily values of the remote sensing input parameters, in the reference semiarid area of the Petrolina County, Brazilian Northeast, are shown in Fig. 4.

A darker land surface, i.e., with a low α_0, absorbs more solar radiation and has a larger available energy than a brighter one, but this also depends on the soil moisture conditions.[16,25,26] The highest α_0 values in the mixed agroecosystems occurred in the image of DOY 265 (September 22), representing the driest period of the year in which the joint effects of low both soil moisture and cloud cover, together with the sun's astronomical position near the zenith position, produce large R_G levels.

However, the α_0 spatial variations were homogeneous along the different periods of the year with standard deviation (SD) of 0.02 in all images, with no strong distinctions among the ICs and NV agroecosystems. Clearly, one can see the largest α_0 values in the southern part of the study area, where the Petrolina city is located, close to the São Francisco River.

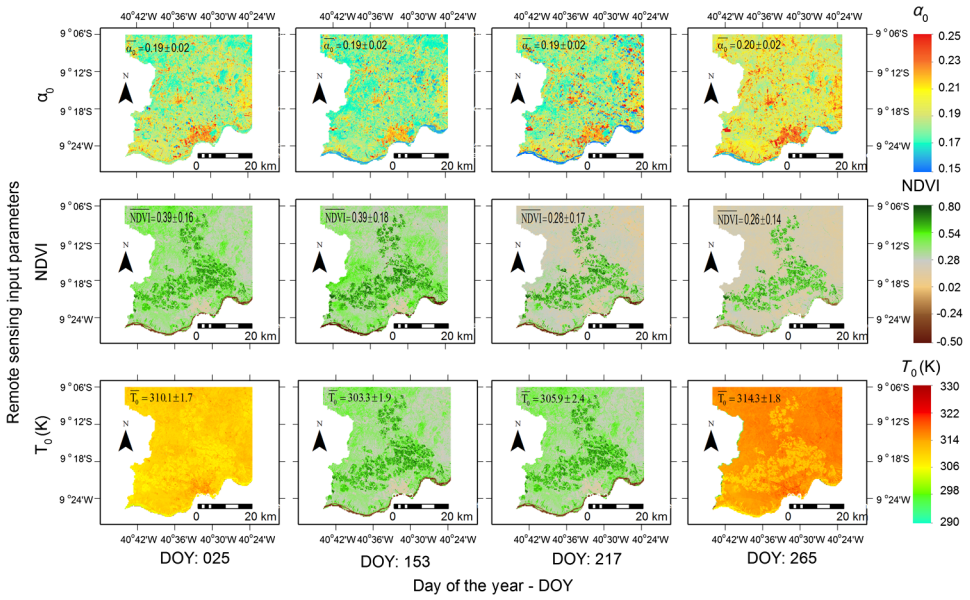

Fig. 4 Spatial distributions of the daily values for the remote sensing modeling input parameters in the reference semiarid area of Petrolina County, Pernambuco, Brazilian Northeast. Surface albedo (α_0), NDVI, and surface temperature (T_0). Overbars mean average pixel values, shown together with the SD.

A similar α_0 range, between 0.15 and 0.26, was reported for tropical NV,[27] but the values found in the current study are higher than those previously reported for humid tropical regions.[28–30] The relation of α_0 with environmental and moisture conditions is also in accordance with other more recent studies.[6,19,25,26,31]

The distinctions among the NDVI large-scale values in the year and among agroecosystems are much clear than in the case of α_0, with the highest differences happening under the driest conditions of the year, at the end of September (DOY 265). On one hand, the largest pixel values are from January to June, represented by the images of DOY 25 and 153 because the NV species ("Caatinga") consume water from the first rains, increasing biomass production (BIO). On the other hand, ICs, besides the rainfall water consumption, are regularly irrigated daily.

As there is a relation between BIO and λE,[32] the water flux rates are higher in ICs than in NV ecosystems. Corn crops presented twice the BIO values when compared with natural alpine meadow in the Heithe River Basin, with irrigation considered the main reason for these strong differences.[33] The lowest large-scale NDVI values were observed in September (DOY 265), when far from the rainy period, the soil in the root zone of the natural species was dry, promoting their senescence stages.

The T_0 parameter affects the energy available by acting in the long wave radiation balance, with its lower values under irrigation conditions than those from the drier areas in the vicinities of irrigated plots. However, even differentiating the agroecosystems better than α_0, these distinctions are not as strong as those promoted by the NDVI pixel values. One reason for this is the lower spatial resolution of the thermal band (100 m) compared with the visible ones (30 m) of the L8 sensor.

In general, the periods with the highest T_0 values coincided with those of the largest R_G levels (DOY 25 and 265, in January and September, respectively). The lowest T_0 occurred in the middle of the year, after the rainy season (DOY 153—June), which is due to the uniform soil moisture in the root zones of the mixed agroecosystems together with the winter solstice time in the south hemisphere.

The variability of α_0, NDVI, and T_0 in the "Caatinga" natural ecosystem can primarily be attributed to variations in R_G and surface moisture conditions due to consequences of the joint effects of sun position, cloud cover, and rainfall. However, for ICs, as the water is in general regularly applied, the magnitudes of these remote sensing parameters are also influenced by the different crop stages together with water and fertilization management.

Table 2 Daily averages of the radiation balance components (RB_{comp}) for the mixed agroecosystems, composed by ICs and NV, under different thermohydrological conditions, in the reference semiarid area inside the Petrolina County, Pernambuco, Northeast Brazil: incident global solar radiation (R_G), reflected solar radiation (R_R), atmospheric emitted longwave radiation (RL_a), and surface emitted longwave radiation (RL_s).

DOY/RB_{comp}	R_G (MJ m^{-2} d^{-1})		R_R (MJ m^{-2} d^{-1})		RL_a (MJ m^{-2} d^{-1})		RL_s (MJ m^{-2} d^{-1})	
DOY	ICs	NV	ICs	NV	ICs	NV	ICs	NV
25	24.13	24.23	4.59	4.61	34.70	34.67	42.87	42.88
153	19.99	19.89	3.69	3.70	32.02	32.01	39.29	39.22
217	19.31	19.20	3.63	3.65	32.96	32.98	39.69	39.65
265	23.92	23.90	4.67	4.81	34.87	34.89	44.16	44.16
Mean	21.84	21.81	4.15	4.19	33.64	33.64	41.50	41.48

Note: DOY, day of the year.

3.3 *Large-Scale Radiation Balance*

Table 2 presents the mean daily pixel values of the radiation balance components (RB_{comp}) for the ICs and NV agroecosystems in the reference semiarid area, involving different thermohydrological conditions in the year 2014 inside the Petrolina County, Brazilian Northeast.

The incident global solar radiation (R_G), considered the direct or indirect (diffuse) radiation from the sun, integrated over all wavelengths in the sw interval, presented seasonal variations in the year 2014, however, with similar values inside the ICs and NV areas. The highest R_G levels occurred in January (DOY 25), during the rainy season, while the smallest ones were in August (DOY 217), during the naturally dry period.

The values of the reflected solar radiation (R_R) followed those for R_G, but R_R was also affected by the soil moisture and soil cover conditions, however, without strong differences among the agroecosystem types. The R_G and R_R accounting gives the sw radiation balance, determining the fraction of solar radiation that is absorbed by the surfaces and converted into heat energy. By several processes, including emission, the surfaces lose this energy as longwave radiation.

The atmosphere absorbs the emitted longwave radiation from the surfaces (RL_s) or loses it into space. In general, RL_s presented seasonal variations, according to R_G levels, but with less dependence on the agroecosystem types when compared with R_R. Part of RL_s finds its way back to the surfaces as emitted longwave radiation from the atmosphere (RL_a).

RL_a is dependent on T_a and on the concentration of carbon dioxide, water vapor, and ozone. RL_s values always stayed above the RL_a ones, by 20% in January (DOY 25) and 27% in August (DOY 217), independent of the surface type. As RL_s was usually greater than RL_a, the net longwave radiation represented an energy loss from the Brazilian semiarid agroecosystems to the lower atmosphere.

Taking into account all components from Table 2, the R_n represents the difference between incoming and outgoing radiation of both short and long wavelengths. The fraction of R_G transformed into R_n ranged from 41% (DOY 217, August) to 47% (DOY 25, January), averaging 45%, independent of the agroecosystem type. This is in agreement with field measurements in ICs and NV done inside the semiarid region of Brazil[16] and with studies involving other agroecosystems,[34,35] giving additional confidence to SAFER for the large-scale radiation and energy balance acquirements by the coupled use of L8 images and agrometeorological stations.

Using R_G and T_a interpolated data together with α_0 on a daily scale, the Slob equation [Eq. (6)] was applied to retrieve the 24-hour large-scale R_n values[7,16,20,21] (Fig. 5).

In general, there were no clear R_n distinctions among irrigated and NV areas and no large spatial differences, with the SDs ranging from 0.6 to 0.9 MJ m^{-2} d^{-1}. Its strongest dependence

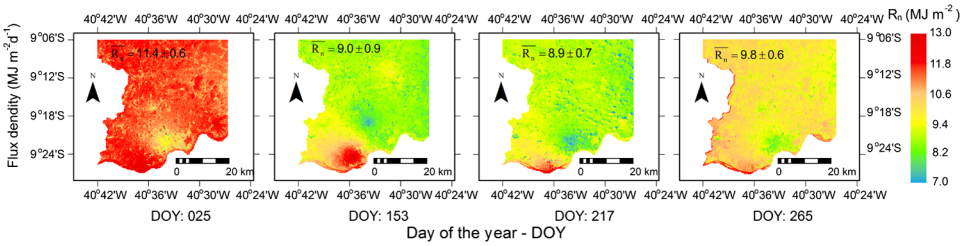

Fig. 5 Spatial distribution of the daily R_n values in the reference semiarid area inside Petrolina County, Pernambuco, Brazilian Northeast. Overbars mean average pixel values, shown together with the SDs.

was on R_G as the largest mean R_n pixel values for January (DOY 25) and September (DOY 265) corresponded to the highest R_G ones (see Fig. 5 and Table 2).

It is clear from Fig. 5 that one cannot classify the R_n values according to the agroecosystem types in the Brazilian semiarid region. Then, spatial differences among ICs and NV should be detected when considering the energy partitions into λE, H, and G, according to the different thermohydrological conditions in the year. These analyses are carried out in Sec. 3.4.

3.4 *Large-Scale Energy Balance*

Acquiring ET through the SAFER algorithm and transforming it into energy units,[6,19] λE was estimated. Considering G to be a fraction of R_n and H retrieved as residue in the energy balance equation, all components of this balance could be spatially determined.[19]

Figure 6 presents the spatial distribution of the daily values for λE, H, and G in the reference semiarid area inside the Petrolina County, Pernambuco state, Northeast of Brazil, for each DOY, involving different thermohydrological conditions in the year 2014.

Clearly, one can distinguish irrigated areas and water bodies from the NV by the highest crop λE pixel values, according to the period of the year, primarily when looking for the image of DOY 265 (September), which represents the climatically driest condition. In some pixels, λE

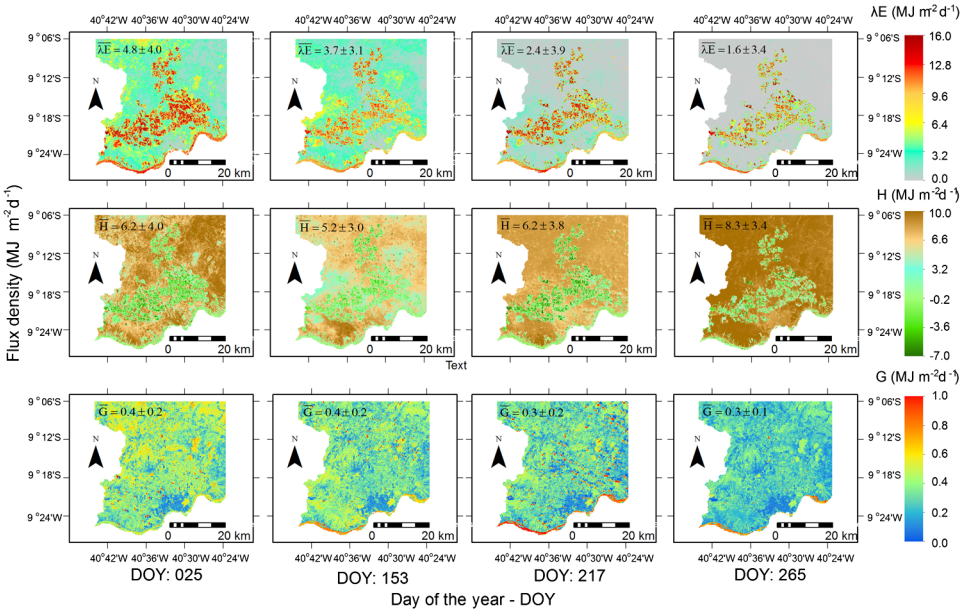

Fig. 6 Spatial distribution of the daily values for the energy balance components in the reference semiarid area inside Petrolina County, Pernambuco, Brazilian Northeast. Latent heat flux (λE), sensible heat flux (H), and ground heat flux (G). Overbars mean average pixel values, shown together with the SDs.

was higher than R_n, representing very well irrigated plots contrasting with the drier vicinity areas (see Figs. 5 and 6). The maximum λE values of 16 MJ m^{-2} d^{-1} return ET rates of 6.5 mm d^{-1}, representing mostly irrigated orchards.

dos Santos et al.,[36] applying SEBAL and S-SEBI algorithms with Landsat images, reported maximum ET values of 6.0 mm d^{-1} in the mixed irrigated and natural agroecosystems under the semiarid Brazilian conditions. Also in a Brazilian semiarid region, but in this case using the METRIC model, Folhes et al.[37] found low values for "Caatinga" (<2.0 mm d^{-1} ~ < 4.9 MJ m^{-2} d^{-1}), moderate values representing orchards (3.0 to 6.0 mm d^{-1} ~ 7.4 to 14.7 MJ m^{-2} d^{-1}), and annual crops with the highest ET rates (>6.0 mm d^{-1} ~ > 14.7 MJ m^{-2} d^{-1}). The main reason for the slightly lower values of these last studies under irrigation conditions could be the image acquisition times, outside the rainy season, which are different from the current study in which the highest λE values were during the rainy period.

During the natural driest conditions of the year, between August and October, represented by the image of DOY 265, NV presented the lowest λE values, while irrigated fields showed the highest ones. Stomata of the natural species were close during this period, limiting transpiration and photosynthesis, while, in general, irrigation intervals in crops are short (daily irrigation), reducing the heat losses to the atmosphere.

The largest large-scale λE values for the mixed agroecosystems were in January (DOY 25) because of the joint effects of rains and irrigation together with high atmospheric demand (see Figs. 3 and 6). During this time of the year, the uniform soil moisture makes "Caatinga" have λE rates similar to those from ICs and even higher in some occasions. Intermediate λE values in NV ecosystem occurred after this period, in June (DOY 153), because the previous rainfalls still kept the natural species actively transpiring.

According to the H spatial variations in Fig. 6, one can also distinguish irrigated areas from the "Caatinga" species by the lowest values in the first ecosystem, with some crop pixel values even being negative, meaning heat horizontal advection from the warmer NV at the vicinities of the irrigated plots, reaching up to −7 MJ m^{-2} d^{-1}. Although with smaller magnitudes, negative H was also measured by eddy covariance system in irrigated orange orchards in the Mediterranean semiarid conditions of Sicily, Italy.[38] The largest H pixels corresponded to the lowest λE values in the image of DOY 265 (September), while the minimum H ones were soon after the rainy period in June (DOY 153), due to low R_G levels and high large-scale soil moisture.

The ground heat flux (G) was the energy balance parameter that presented the lowest spatial variations among the Brazilian semiarid agroecosystems. Its values were very low, confirming that in most cases under semiarid conditions, they approach to zero at the daily scale,[6,16,39] and could be neglected at this time-scale, as few areas presented daily values reaching up to around 1.0 MJ m^{-2} d^{-1}.

Regarding the spatial variations, the lowest SD values for λE and H were soon after the rainy season. Under these conditions, the soil moisture in the root zone of all agroecosystems was high, but with all of them under low R_G levels (see Figs. 3 and 6), situation represented by image of DOY 153 (June 2014).

Vegetation was classified into ICs and NV agroecosystems by applying the SUREAL algorithm [Eq. (17)] and the r_s thresholds.[24]

Table 3 shows the daily average energy balance components together the evaporative fraction [$E_f = \lambda E/(R_n - G)$] for ICs and NV, under different thermohydrological conditions in the reference semiarid region inside Petrolina County, Pernambuco, Northeast Brazil.

The lowest R_n and λE average pixel values for the ICs agroecosystem were at the start of August (DOY 217), while the highest R_n average was during the rainy period (DOY 25) and the one for λE occurred inside the climatically driest conditions represented by the image of DOY 265 (September). The λE and R_n values produced a mean E_f range from 0.66 to 0.81, respectively, evidencing good soil moisture conditions in the root zone of the irrigated fruit crops. Consoli and Papa,[38] using field energy balance techniques with eddy covariance data, in irrigated orange orchards in the Mediterranean conditions, found a slightly lower average $\lambda E/R_n$ of 0.62, when comparing with the current study. Bezerra et al.,[39] applying the Bowen ratio method in irrigated cotton crop in the Brazilian semiarid conditions, found values of $\lambda E/R_n$ ranging from 0.58 to 0.81, similar to our results for ICs (from 0.63 to 0.79, averaging 0.70).

Table 3 Daily averages of the energy balance components for the mixed agroecosystems inside the reference semiarid area of Petrolina County, Pernambuco, Northeast Brazil: net radiation (R_n), latent heat flux (λE), sensible heat flux (H), soil heat flux (G), and the evaporative fraction $\{E_f = [\lambda E/(R_n - G)]\}$.

DOY/mean	R_n (MJ m^{-2} d^{-1})		λE (MJ m^{-2} d^{-1})		H (MJ m^{-2} d^{-1})		G (MJ m^{-2} d^{-1})		E_f (-)	
DOY	ICs	NV	ICs	NV	ICs	NV	ICs	NV	ICs	NV
25	11.33	11.29	7.77	4.25	3.21	6.77	0.39	0.39	0.71	0.39
153	9.02	9.05	6.32	3.22	2.35	5.41	0.36	0.35	0.73	0.37
217	8.97	9.08	5.69	1.75	2.91	6.80	0.35	0.33	0.66	0.20
265	10.02	9.26	7.88	0.36	1.79	9.20	0.29	0.26	0.81	0.04
Mean	9.84	9.67	6.92	2.40	2.57	7.05	0.35	0.33	0.73	0.25

Note: ICs, irrigated crops; NV, natural vegetation; and DOY, day of the year.

Considering the NV ecosystem, the periods with the highest and the lowest mean R_n values were the same of that for ICs, but for λE the smallest average happened in September (DOY 265), with the E_f in this natural ecosystem ranging between 0.04 and 0.39. The characteristics of the "Caatinga" natural species were manifested by low values of both λE and E_f, outside the rainy season. For ICs, the largest E_f happened on occasions of heat advection from their surrounding natural drier areas.

Considering the whole year, H mean pixel value for the NV ecosystem was almost three times larger than that for ICs. On average, H reached 99% of R_n in September (DOY 265) for the first ecosystem, while the corresponding fraction for ICs was only 18% during this period. The average H/R_n under the Mediterranean conditions[38] of 30% was almost the same as the current study (26%). The range of H/R_n from 18 to 28% for the ICs agroecosystem is inside the values reported by Bezerra et al.[39] for ICs under the semiarid conditions of the Northeast Brazil (11 to 29%).

Despite G values of up to 1.0 MJ m^{-2} d^{-1} (see Fig. 6) in some areas, the 24-hour averages for both ICs and NV ecosystems were very low, with daily G/R_n fractions ranging from only 3% to 4%, with no perceptible spatial distinctions along the seasons among either agroecosystem. On one hand, Bezerra et al.[39] reported G/R_n daily values ranging as high as 15% in irrigated cotton crops under the Brazilian semiarid conditions. On the other hand, Consoli and Papa[38] found lower 24-hour average G/R_n of 0.01 in irrigated orange orchards in the Mediterranean semiarid climate. However, the daily fractions in the current study are in agreement with field measurements carried out by Teixeira et al.[16] involving irrigated orchards and NV in the current study area. These G/R_n differences could be due to different soil covers.

For the whole year of 2014, in average, the ratios R_n/R_G, $\lambda E/R_n$, H/R_n, and G/R_n were 0.45, 0.70, 0.26, and 0.04, respectively, for the ICs ecosystem, while the corresponding ratios for the NV ecosystem were 0.45, 0.25, 0.72, and 0.03, respectively. The knowledge of these fractions is relevant to considering the land-use change effects, together with climate alterations and water scarcity.

The field eddy covariance and Bowen ratio measurements in ICs and NV in the study area previously done by Teixeira et al.[16] returned respectively mean E_f values of 0.80 and 0.30, which are close to the average pixel values shown in Table 3 by applying the SAFER and SUREAL algorithms. The similarities of our large-scale results with field measurements in the study area and others from literature are encouraging, stimulating the use of these algorithms with the L8 satellite for quantifying the land-use effects on the energy exchanges in semiarid environments.

4 Conclusions

The joint use of L8 images and agrometeorological stations allowed the quantification and analyzes of the 24-hour radiation and energy balance components on large-scales in the year 2014,

under different thermohydrological semiarid conditions in the Petrolina County, Pernambuco state, Northeast Brazil. R_n was more strongly influenced by the solar radiation levels than by the characteristics of the different agroecosystems types, but the water and vegetation conditions were well identified from the energy partition patterns. It was demonstrated that the daily values of the latent (λE), sensible (H), and ground (G) heat fluxes can be estimated for ICs and NV from instantaneous measurements of the visible, near-infrared, and thermal radiations from the L8 sensor, through the application of the SAFER and SUREAL algorithms. The mean fractions of λE, H, and G to R_n were 70%, 26%, and 4%, and 25%, 72%, and 3%, for ICs and NV agroecosystems, respectively. In some occasions, in well irrigated ICs, heat fluxes were evidenced coming from the NV dryer areas at their vicinities, promoting λE higher than R_n and negative H values. The large-scale analyses of the energy and mass exchange dynamics can contribute to the monitoring of the land-use and climate changes effects in the Brazilian semiarid region. The modeling success here gives more confidence for using the algorithms with L8 images together with weather stations in other semiarid environments around the world, which probably will need only calibrations of the original equations.

References

1. A. H. de C. Teixeira, "Determining regional actual evapotranspiration of irrigated and natural vegetation in the São Francisco river basin (Brazil) using remote sensing and Penman–Monteith equation," *Rem. Sens.* **2**, 1287–1319 (2010).
2. D. G. Miralles et al., "Global land-surface evaporation estimated from satellite-based observations," *Hydrol. Earth Syst. Sci.* **15**, 453–469 (2011).
3. M. C. Anderson et al., "Mapping daily evapotranspiration at Landsat spatial scales during BEAREX'08 field campaign," *Adv. Water Res.* **50**, 162–177 (2012).
4. I. Pôças et al., "Using remote sensing energy balance and evapotranspiration to characterize Montane landscape vegetation with focus on grass and pasture lands," *Int. J. Appl. Earth Obs. Geoinf.* **21**, 159–172 (2013).
5. R. G. Allen et al., *Crop Evapotranspiration: Guidelines for Computing Crop Water Requirements*, Food and Agriculture Organization of the United Nations, Rome, Italy (1998).
6. A. H. de C. Teixeira et al., "A comparative study of techniques for modeling the spatio-temporal distribution of heat and moisture fluxes in different agroecosystems in brazil," in *Remote Sensing of Energy Fluxes and Soil Moisture Content*, G. G. Petropoulos, Ed., 1st ed., pp. 169–191, CRC Group, Taylor and Francis, Boca Raton, Florida (2014).
7. W. G. M. Bastiaansssen et al., "A remote sensing surface energy balance algorithm for land (SEBAL) 1. Formulation," *J. Hydrol.* **212–213**, 198–212 (1998).
8. G. J. Roerink, Z. Su, and M. Menenti, "S-SEBI: a simple remote sensing algorithm to estimate the surface energy balance," *Phys. Chem. Earth* **25**, 147–157 (2000).
9. Z. Su, "The surface energy balance system (SEBS) for estimation of turbulent heat fluxes," *Hydrol. Earth Syst. Sci.* **6**, 85–100 (2002).
10. A. H. de C. Teixeira et al., "Reviewing SEBAL input parameters for assessing evapotranspiration and water productivity for the low-middle São Francisco River basin, Brazil: part A: calibration and validation," *Agric. For. Meteorol.* **149**, 462–476 (2009).
11. A. H. de C. Teixeira et al., "Reviewing SEBAL input parameters for assessing evapotranspiration and water productivity for the low-middle São Francisco River basin, Brazil: part B: application to the large scale," *Agric. For. Meteorol.* **149**, 477–490 (2009).
12. H. A. Cleugh et al., "Regional evaporation estimates from flux tower and MODIS satellite data," *Remote. Sens. Environ.* **106**, 285–304 (2007).
13. P. L. Nagler et al., "Estimating riparian and agricultural actual evapotranspiration by reference evapotranspiration and MODIS enhanced vegetation index," *Remote Sens.* **5**, 3849–3871 (2013).
14. B. Kamble, A. Kilic, and K. Hubard, "Estimating crop coefficients using remote sensing-based vegetation index," *Remote Sens.* **5**, 1588–1602 (2013).
15. R. G. Allen et al., "Satellite-based energy balance for mapping evapotranspiration with internalized calibration (METRIC)—Applications," *J. Irrig. Drain. Eng.* **133**, 395–406 (2007).

16. A. H. de C. Teixeira et al., "Analysis of energy fluxes and vegetation-atmosphere parameters in irrigated and natural ecosystems of semi-arid Brazil," *J. Hydrol.* **362**, 110–127 (2008).
17. F. B. T. Hernandez et al., "Determining large scale actual evapotranspiration using agrometeorological and remote sensing data in the Northwest of Sao Paulo State, Brazil," *Acta Hortic.* **1038**, 263–270 (2014).
18. Q. Vanhellemont and K. Ruddick, "Turbid wakes associated with offshore wind turbines observed with Landsat 8," *Remote Sens. Environ.* **145**, 105–115 (2014).
19. A. H. de C. Teixeira et al., "Energy balance with Landsat images in irrigated central pivots with corn crop in the São Paulo State, Brazil," *Proc. SPIE* **9239**, 92390O (2014).
20. A. H. de C. Teixeira, *Water Productivity Assessments from Field to Large Scale: A Case Study in the Brazilian Semi-Arid Region*, Lambert Academic Publishing, Saarbrücken, Germany (2009).
21. H. A. R. de Bruin and J. N. M. Stricker, "Evaporation of grass under non-restricted soil moisture conditions," *Hydrol. Sci.* **45**, 391–406 (2000).
22. R. G. Allen, O. Hartogensis, and H. A. R. de Bruin, "Long-wave radiation over alfafa during the RAPID field campaign in southern Idaho," Research Report, University of Idaho, Kimberly (2000).
23. M. R. Raupasch, "Combination theory and equilibrium evaporation," *Q. J. R. Meteorol. Soc.* **127**, 1149–1181 (2001).
24. A. H. de C. Teixeira, "Determination of surface resistance to evapotranspiration by remote sensing parameters in the semi-arid region of Brazil for land-use change analyses," C. M. U. Neale and M. H. Cosh, Eds., 1st ed., Vol. **352**, pp. 167–170, IAHS Press, Wallingford, United Kingdom (2012).
25. S.-G. Li et al., "Energy partitioning and its biophysical controls above a grazing steppe in central Mongólia," *Agric. For. Meteorol.* **137**, 89–106 (2006).
26. A. I. J. M. van Dijk, L. A. Bruijnzeel, and J. Schellekens, "Micrometeorology and water use of mixed crops in upland West Java, Indonesia," *Agric. For. Meteorol.* **124**, 31–49 (2004).
27. J. L. Monteith and M. H. Unsworth, *Principles of Environmental Physics*, Arnold, London (1990).
28. J. S. Oguntoyinbo, "Reflection coefficient of natural vegetation, crops and urban surfaces in Nigeria," *Q. J. R. Meteorol. Soc.* **96**, 430–441 (1970).
29. R. T. Pinker, O. E. Thompson, and T. F. Eck, "The albedo of a tropical evergreen forest," *Q. J. R. Meteorol. Soc.* **106**, 551–558 (1980).
30. W. J. Shuttleworth, "Evaporation from Amazonian rain forest," *Proc. R. Soc. London Biol. Sci.* **233**, 321–346 (1988).
31. D. B. Lobell and G. P. Asner, "Moisture effects on soil reflectance," *Soil Sci. Soc. Am. J.* **66**, 722–727 (2002).
32. M. Yuan et al., "Assessment of crop growth and water productivity for five C3 species in the semi-arid Inner Mongolia," *Agric. Water Manage.* **122**, 28–38 (2013).
33. M. Wang et al., "Vegetation primary production estimation at maize and alpine meadow over the Heihe River Basin, China," *Int. J. Appl. Earth Obs. Geoinf.* **17**, 94–101 (2012).
34. I. A. M. Yunusa, R. R. Walker, and P. Lu, "Evapotranspiration components from energy balance, sapflow and microlysimetry techniques for an irrigated vineyard in inland Australia," *Agric. For. Meteorol.* **127**, 93–107 (2004).
35. C. E. Hughes et al., "Estimating evapotranspiration for a temperate salt marsh Newcastle, Australia," *Hydrol. Process* **15**, 957–975 (2001).
36. C. A. C. dos Santos et al., "Assessment of daily evapotranspiration with SEBAL and S-SEBI algorithms in cotton crop," *Rev. Brasil. Meteorol.* **25**, 383–392 (2010).
37. M. T. Folhes, C. D. Rennó, and J. V. Soares, "Remote sensing for irrigation water management in the semi-arid Northeast of Brazil," *Agric. Water Manage.* **96**, 1398–1408 (2009).
38. S. Consoli and R. Papa, "Corrected surface energy balance to measure and model the evapotranspiration of irrigated orange orchards in semi-arid Mediterranean conditions," *Irrig. Sci.* **31**, 1159–1171 (2013).
39. B. G. Bezerra et al., "Surface energy exchange and evapotranspiration from cotton crop under full irrigation conditions in the Rio Grande do Norte State, Brazilian Semi-Arid," *Bragantia* **74**, 120–128 (2015).

Antônio Heriberto de Castro Teixeira is a researcher at Embrapa Satellite Monitoring. He received his BS degree in agronomy from Pernambuco Federal Rural University in 1988, his MS degree in meteorology from Paraíba Federal University in 1993, and his PhD in environmental sciences from Wageningen University in 2008. He is the author of more than 55 journal papers and has written one book and 23 book chapters. His current research interests include radiation and energy balances, evapotranspiration, biomass production, water productivity, and agrometeorological indices.

Janice Freitas Leivas is a researcher at Embrapa Satellite Monitoring. She received her BS degree in meteorology at the Federal University of Pelotas (UFPEL) in 2003 and her MS degree in agricultural climatology statistics at Federal University of Rio Grande do Sul (UFRGS) in 2003, and her PhD in agrometeorology, at UFRGS in 2008. Her actual research activities are concentrated on remote sensing applications.

Fernando Braz Tangerino Hernandez graduated in agronomic engineering in 1987 and received his MS degree in agronomy (vegetal production) at the São Paulo State University–UNESP in 1987 and PhD in irrigation and drainage from Superior Luiz de Queiroz-USP in 1995. Currently, he is a senior professor at UNESP. He has experience on agricultural engineer, with emphasis on irrigation and drainage, mainly in the following research fields: irrigated agriculture, agrometeorology, and hydrology.

Renato Alberto Momesso Franco is a biologist and has BS, MS and PhD degrees from the São Paulo State University. He has been working as a researcher with emphasis on water resources, remote sensing and geographic information systems.